Original Article

Institution of MECHANICAL ENGINEERS
Journal of ENGINEERING TRIBOLOGY

Thermal interactions in rolling bearings

Proc IMechE Part J:
J Engineering Tribology
2020, Vol. 234(8) 1233–1253

DOI: 10.1177/1350650119886234
journals.sagepub.com/home/pij
SAGE

Pradeep K Gupta[1], Jared I Taketa[2] and Craig M Price[2]

Abstract

Rolling bearing dynamics model, based on classical differential equations of motion of bearing elements coupled with thermal interactions, is presented. While churning and drag effects are based on classical laminar and turbulent flow theories, independently measured lubricant rheology, including shear dependence of viscosity, is used to model lubricant traction. The energy equation is integrated through the lubricant film to first compute Newtonian traction with thermal effects. Viscosity dependence on shear stress is then applied to model "shear-thinning" effects. At very high contact pressure and very low slide-to-roll ratios material creep effects, where the behavior of lubricated and dry contacts is similar, are implemented, while a shear stress limit is applied at very high slide-to-roll ratios. Traction predictions for a typical contact in a traction rig show good agreement with experimental traction data. Transient heat generations are time-averaged over thermal time step to compute time-varying temperature fields in the bearing, which alter properties of bearing materials, operating bearing geometry, and rheology of the lubricant. As the transient solutions converge to stable operating temperatures, bearing heat generation approaches the expected steady-state value. Heat generation predictions for both ball and rolling bearings are in good agreement with measured experimental data.

Keywords

Rolling bearing dynamics, thermal stability, heat generation in rolling bearings, lubricant traction, frictional interactions, Advanced Dyanamics of Rolling Elements (ADORE)

Date received: 15 April 2019; accepted: 9 October 2019

Introduction

Thermal interactions in a rolling bearing very often control the overall performance of rolling bearings. The heat generated between interacting bearing elements travels through the bearing to the support system and in the process, alters the temperature field in the bearing. The changes in operating temperatures affect internal geometry, material properties, and lubricant behavior, all of which alter interactions between bearing elements to modify the bearing load distribution, lubricant traction, and overall bearing element motion; the altered bearing interactions, in turn, affect heat generation. Such an intricately coupled process continues until all solutions converge to steady-state conditions. In the event, stable steady-state solutions cannot be reached, the bearing experiences a thermal instability and failure is eminent. Thus, realistic thermal modeling is a key element in the development of bearing performance simulation models.

Lubricant churning and drag and frictional interactions between the bearing elements essentially constitute the sources of heat generation in rolling bearings. In high-speed rolling bearings with circulating lubricant, such as those used in turbine engines, the heat generated due to lubricant churning and drag often constitutes the majority of total bearing heat generation. Modeling of these effects requires definition of fluid flow patterns within the bearing, which is an extremely complicated task and it often requires a number of simplifying assumptions. Aside from properties of the churning media, the primary input to modeling of these effects is the velocity of bearing elements as they move within the bearing and shear through the lubricant in the bearing cavity. Both the orbital and angular velocities of rolling elements may be well estimated by simple bearing kinematics as formulated in quasi-static solutions by Jones.[1] Although the quasi-static equilibrium analysis requires certain empirical kinematic hypothesis, such as race control, the analysis does provide a fairly good estimate of the rolling element velocities. With regard to the cage, although the interactions between both rolling element and cage, and race and cage, are highly dynamic, the assumption that the cage angular velocity is equal

[1]PKG Inc., Clifton Park, USA
[2]Rolls-Royce Corporation, Indianapolis, USA

Corresponding author:
Pradeep K Gupta, Pradeep K Gupta Inc. (PKG Inc.), 117 Southbury Road, Clifton Park, NY 12065, USA.
Email: guptap@pradeepkguptainc.com

to the average rolling element orbital velocity is a fairly good one. Using these assumptions and the quasi-static bearing analysis, Rumbarger et al.[2] formulated simple equations to compute the drag forces on rolling elements and churning moments on both the rolling elements and cage; the formulation is based on classical laminar and turbulent flow theories, as documented by Schlichtig.[3] In view of the complexities associated with fluid flow in the bearing, this simplified formulation is still considered as state-of-the-art in modeling churning and drag effects. Crecelius and Pirvics,[4] in the development of bearing code, SHABERTH, presented empirical estimates for effective density of the lubricant, when only a part of the bearing cavity is filled with oil, to estimate the churning and drag effects from the simplified churning and drag models. For high-speed rolling bearings with circulating lubricant, Parker[5] presented fairly good experimental validation of bearing heat generation as provided by the SHABERTH.

Since the bearing element velocities, as computed by kinematic hypothesis used in quasi-static solutions, are relatively insensitive to applied load on the bearing, bearing heat generations as simulated by quasi-static models show little or no load dependence. Although in angular contact ball bearings the operating contact angles do have a load dependence, the small change in kinematic velocities resulting from the altered contact angles do not show a notable effect on the churning and drag losses. Thus, when churning and drag losses constitute majority of overall bearing heat generation, the heat generation predictions by the quasi-static models remain relatively insensitive to load. Recently, Forster et al.,[6,7] while presenting an empirical bearing heat generation model for a 133 mm bore angular contact ball bearing in terms of a simple correlation between experimentally measured heat generation and several operational variables, have demonstrated that heat generation predicted by SHABERTH is relatively insensitive to applied load. Subsequent to this work, Nicholson et al.[8] used ADORE[9] to demonstrate that the dynamic model, which includes effect of lubricant traction, does show a load dependence of bearing heat generation. In other words, the load dependence of bearing heat generation is correlated to lubricant traction.

In addition to applied load, thermal dissipations in frictional interactions are also sensitive to subtle variations in slip velocities in the rolling element to race contacts. Although under moderate loads (Hertz contact stress less than 1.5 GPa) the heat generated in frictional interactions may be a small part of the total bearing heat generation, these interactions are known to be principal contributors to stability of motion of both rolling elements and cage at all operational speeds. As both the applied load and operating speed increase, the frictional dissipations also increase and they become comparable to those in lubricant churning and drag effects. However, relative slip between interacting bearing elements, which is a key input in modeling frictional interactions, may only be defined by time variation in bearing element velocities. For a realistic simulation of the slip velocities, it is therefore essential to carry out a truly dynamic simulation where the equilibrium equations for the bearing elements in quasi-static bearing models, such as SHABERTH, are replaced by differential equations of motion, which are integrated in time to determine steady-state behavior of the bearing. Walters[10] developed such a formulation of motion for the cage in an angular contact ball bearing to investigate cage instabilities. In this work, motion of the balls, however, remained constrained to the equilibrium equations. Subsequently, Gupta[11] formulated the differential equations for ball motion to investigate skid in a ball bearing in real-time, and later presented generalized dynamic formulations for both ball and roller bearings,[12] which included equations of motion for both rolling elements and cage. These works led to the presently well distributed bearing dynamics code ADORE.[9] Subsequent to ADORE development, there have been number of other advances in both quasi-static and dynamic modeling of rolling bearings. An extensive review of these developments has been compiled by Gupta.[13]

Once the relative slip at the rolling element to race contacts is determined, the lubricant behavior in the contact becomes significant in defining the applicable friction or traction force responsible for overall rolling element motion and frictional dissipation in the contact. This prompted extensive research on lubricant rheology and traction behavior in concentrated elastohydrodynamic contacts. Formulation of and solution to the generalized lubricant flow equations, with the pressure and temperature dependent properties, is an extremely complex task, and practical implementation of such formulations in rolling bearing performance models becomes relatively impractical from both numerical and computational stand points. With due recognition of such difficulties, Kannel and Walowit[14] presented a simplified traction model based on Newtonian behavior of the lubricant with prescribed viscosity–pressure–temperature relations. With lack of experimental techniques for lubricant rheology measurements at the time, the model was fitted to experimental traction-slip data to estimate the constitutive coefficients in arbitrarily selected viscosity–pressure–temperature relations.[15] Unlike the Newtonian behavior, Johnson and Tevaarwerk[16] introduced a visco-elastic model, where in addition to viscosity, lubricant traction is based on shear modulus and a critical shear stress associated with the lubricant. Again, due to lack of experimental capabilities for the measurement of applicable shear modulus and critical shear stress, Gupta et al.[17] carried out a regression analysis of experimental traction data to estimate the applicable coefficients in the Johnson–Tevaarwerk model.

Traction predictions with constitutive constants derived from experimental traction data are limited to the operational limits of available traction rigs while the operating conditions in typical turbine engine bearings are beyond such limits. For example, the rolling velocity in traction rigs is, generally, limited to about 25 m/s, whereas the rolling velocity in turbine engine bearings could be as high as 80 m/s. Likewise, there are pressure and temperature limitations as well. These limitations imply that traction predictions in turbine engine bearing environment cannot be validated in available traction rigs. Hence traction modeling in such bearings must rely on significant extrapolation of operating conditions under which the traction models are developed. The uncertainties associated with such extrapolations emphasize the fact that the model must be based on physical behavior rather than simple regression of experimental traction data which essentially curve fits the model to derive the constitutive coefficients. In more recent years, Bair[18] has developed more advanced experimental techniques to measure lubricant viscosity not only as a function of pressure and temperature, but also as a function of shear stress. It has been proposed that the lubricant viscosity reduces with shear stress, which has led to a "shear-thinning" model. With the advancements in experimental techniques for measurement of lubricant rheology, it has also been demonstrated that traction predictions in elastohydrodynamics contacts in rolling bearings over a wide range of operating conditions are now possible by independently measured lubricant rheology.

With the above advancements, the objective of this investigation is to enhance the current rolling bearing dynamics model to predict heat generation in the bearing, based on temperature dependent properties of bearing materials and lubricants. The primary emphasis is on high-speed turbine engine applications where the bearings are lubricated with circulating oil. The modeling approach is schematically described in Figure 1. Fundamental material behavior, applicable geometrical compatibility requirements under prescribed operating conditions, and governing equations for the interactions being modeled constitute the basic elements of the model. Bearing heat generations and overall bearing performance predictions are then validated against independently measured experimental data. The approach applies to all interactions in the bearing, including traction, lubricant churning and drag, and the resulting thermal interactions in the bearing. Note that the experimental data have no input in model development and it is only used to validate the model predictions.

The model is based on the existing bearing dynamics code, ADORE,[9] which provides the general framework for the formulation and integration of classical differential equations of motion of bearing elements. Lubricant traction model is based on measured lubricant rheology and the available traction data are only used to validate model predictions. The measured lubricant viscosity data are also used for modeling the churning and drag effects. A thermal interaction model, based on conductive and convective modes of heat transfer, is developed to compute time-varying temperature fields in the bearing, which provide appropriate time variation in operating bearing geometry and material properties. As the time-varying solutions converge to steady-state solutions, the expected steady-state bearing heat generation is predicted and validated against independently measured heat generation data. Typical turbine engine ball and roller bearings with the common MIL-L-23699 lubricant, for which experimental data are presently available, are considered as examples to validate the model predictions.

While the primary emphasis in the present investigation is on high-speed, high-load turbine engine

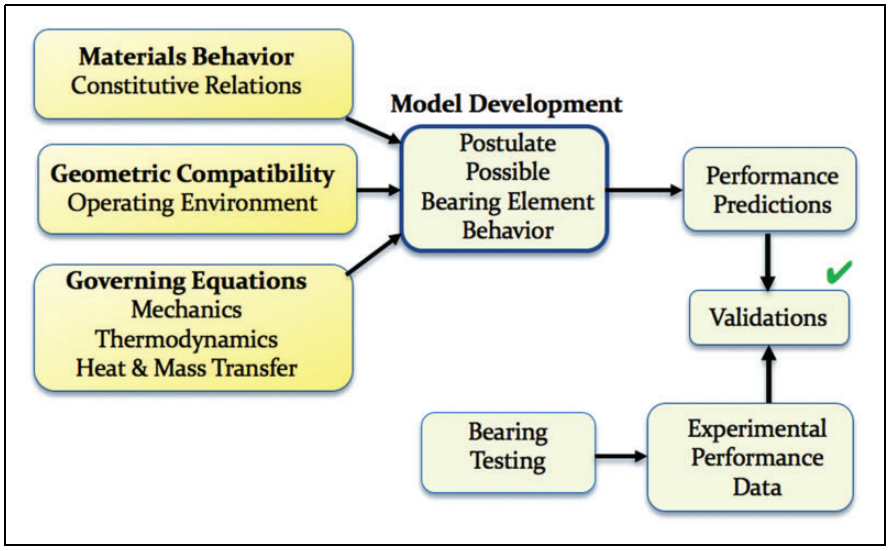

Figure 1. Schematic description of model development based on independently measured constitutive behavior.

applications, the model, to some extent, may also be applied to the more common grease lubricated rolling bearings by using the base stock of the grease as the primary lubricant. Since grease is essentially a semi-solid consisting of a solution of soap and the base stock oil, the initial viscosity is quite high. However, as the bearing element shears through the grease, most of the soap is pushed aside and the applicable viscosity reduces to that of the base stock oil. Hence the assumption of using the base stock as primary lubricant for the concentrated rolling element and race contacts is fairly reasonable. For churning and drag losses, however, the soap may provide additional resistance to the motion of bearing elements. Such a resistance is not considered in the present model. Aside from this limitation, the model may be applicable to any rolling bearing application with a defined traction model for the rolling element to race contacts, and a specified circulating fluid the properties of which determine the churning and drag losses.

Lubricant viscosity

The fundamental lubricant property input to an elastohydrodynamic traction model is the lubricant viscosity as a function of pressure and temperature. Recent advances in high-pressure viscometers[18,19] have provided reliable viscosity measurements at pressures exceeding 1 GPa. Furthermore, regression fit to Yasutomi-type correlation,[20] based on the work of Williams et al.,[21] has provided greatly improved viscosity model. More recent work by Bair et al.[22] has greatly improved the viscosity–pressure–temperature relation by introducing the relative thermal expansivity of free volume in the Yasutomi correlation. Based on measured lubricant rheology these advances have led to reliable traction predictions under arbitrary operating environments.

In the present investigation, experimentally measured viscosity data[18] for the MIL-L-23699 type lubricant are fitted to the improved Yasutomi–Bair correlation, as developed by Bair et al.[22] The applicable relationship is written as

$$\mu = \mu_g \exp\left[\frac{-2.303C_1(T - T_g)F}{C_2 + (T - T_g)F}\right] \text{ Pa.s} \tag{1a}$$

$$T_g = T_{go} + a_1 \ln(1 + a_2 p)\ ^\circ\text{C} \tag{1b}$$

$$F = (1 + b_1 p)^{b_2} \quad 1/^\circ\text{C} \tag{1c}$$

where μ is the viscosity (Pa s) at pressure p (GPa) and temperature T (°C), and the various constants are expressed as

$\mu_g = 10^{12}$ Pa.s (the glass transition viscosity)

$T_{go} = -85.6142427\,^\circ$C (the reference glass transition temperature)

$a_1 = 5423.058449\,^\circ$C

$a_2 = 0.01021915$ 1/GPa

$b_1 = 12.90208578$ 1/GPa

$b_2 = -0.388203465$

$C_1 = 15.84407875$

$C_2 = 18.73143717$

Fit of the above correlation to the experimental viscosity data for MIL-L-23699 data is shown in Figure 2.

The currently used traction models[14,15] employ a simple exponential viscosity–pressure–temperature relation of the type

$$\mu = \mu_o \exp\left[\alpha p + \beta\left(\frac{1}{T} - \frac{1}{T_o}\right) + \gamma p\left(\frac{1}{T} - \frac{1}{T_o}\right)\right] \tag{2}$$

where the constitutive coefficients are derived by a regression fit of the model to the experimental viscosity data

Reference temperature, $T_o = 300$ K

Reference viscosity, $\mu_o = 0.057044$ Pas

Pressure–viscosity coefficient, $\alpha = 1.0964 \times 10^{-8}$ 1/Pa

Temperature–viscosity coefficient, $\beta = 2864.9$ K

Pressure–temperature–viscosity coefficient, $\gamma = 5.9581 \times 10^{-6}$ K/Pa

For the purpose of viscosity prediction at arbitrary temperature and pressure, significance of the Yasutomi–Bair correlation against the simple exponential relation is tested by computing a coefficient of determination, which is a statistical measure of extent of variance in viscosity related to the variance in input pressure and temperature. This coefficient is commonly denoted as R^2; a value of 1 implies that 100% of variation in viscosity is contained in the variation in input pressure and temperature, and the model prediction is best. This coefficient of determination with the Yasutomi–Bair relation, equation (1), is compared with that computed from the simple exponential type relation, equation (2), in Figure 3. Clearly the Yasutomi–Bair correlation provides a coefficient of determination very close to 1.0 over the entire range of temperatures, indicating that the model fit is close to best possible. This implies the Yasutomi–Bair relation contains essentially all the variation in viscosity in terms of pressure and temperature variations. Aside from viscosity prediction, the model fits very well to the slopes in Figure 2, which permits reliable prediction of viscosity, and therefore traction, at turbine engine operating conditions, which are far beyond the experimental limitations on any traction rig. Somewhat notable reduction in coefficient of determination at the high temperature is due to significantly reduced number of experimental data points at this temperature.

Simplified Newtonian traction

Since traction in a rolling/sliding elastohydrodynamic contact produces heat, which in turn affects the

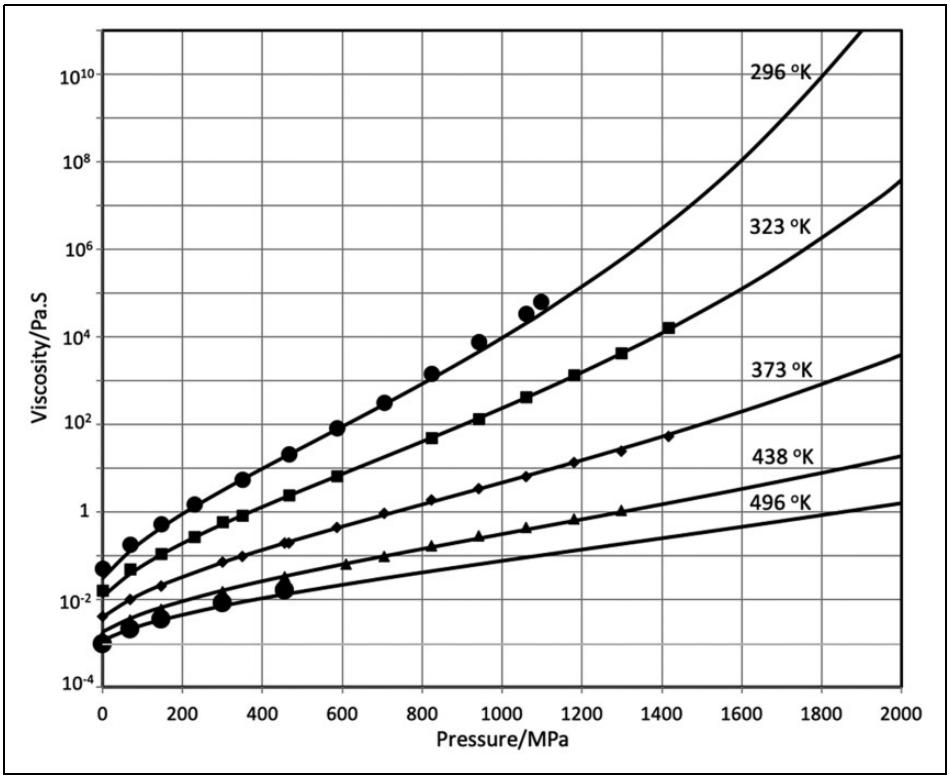

Figure 2. Improved Yasutomi–Bair correlation for MIL-L-23699 lubricant.

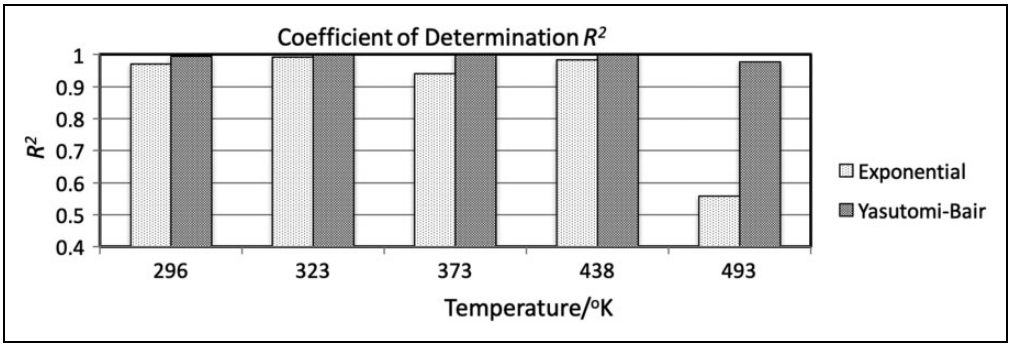

Figure 3. Comparison of coefficient of determination between Yasutomi–Bair and exponential viscosity models.

lubricant viscosity, a treatment of thermal effects is essential in a traction model. In addition, since modeling of thermal effects requires specific heat and thermal conductivity, which may also depend on pressure and temperature, the temperature and pressure variation of these properties must also be considered. With due consideration of dependence of all the fundamental properties of the lubricant on pressure and temperature, fairly complex numerical solutions, with adequate validation against experimental data, have been obtained during the last decade.[23–25] Also, the influence of viscosity dependence on shear stress, as extensively documented by Bair,[18] has been modeled in fair detail.[26] Although for a single contact with prescribed slide-to-roll ratio these solutions present fairly rigorous modeling of traction in concentrated contacts, the numerical complexities associated with the models present several limitations in adopting these solutions to actual rolling bearing performance simulation tools. First, in rolling element to race contacts in a rolling bearing, in addition to pressure and temperature variation over the contact, the slip rates also vary significantly. This requires the contact zone to be segmented in several elementary elements and the traction model be applied on each element and subsequently integrated over the contact to compute total traction. Then the computation has to be repeated for inner and outer race contacts and then there a number of rolling elements in the bearing. Furthermore, in real-time dynamic bearing performance simulation, each contact in the bearing has to be analyzed millions of times. Therefore, for practical

effectiveness of bearing performance simulation tools, the traction model should be simple yet predict realistic lubricant behavior. For these reasons, traction model development in the present investigation is greatly simplified: first, with a prescribed viscosity–pressure–temperature relation Newtonian traction is computed and then appropriate modification to computed traction is applied to simulate non-Newtonian effects such as shear stress effects on viscosity, or "shear-thinning." Model credibility is then established by validating traction predictions in a prescribed contact against independently measured traction data in a traction rig. It should be emphasized that unlike the earlier approaches, the experimental traction data have no input in traction model development; the data are only used to validate predictions of the model under the operating conditions applicable to the traction rig.

The approach to computation of Newtonian traction is essentially identical to the simplified model presented by Kannel and Walowit.[14] However, the very simple exponential type viscosity–pressure–temperature relation is replaced by the above Yasutomi–Bair correlation for greatly improved viscosity prediction. Consider the schematic description of a rolling/sliding contact at a ball to race contact as shown in Figure 4. For most ball bearings, the contact ellipse is fairly narrow; the ratio of major to minor axis of the contact ellipse is greater than 5. Thus, slip variations along the minor axis may be ignored and the contact may be treated as a line contact similar to that in a roller bearing. Then, using a numerical quadrature algorithm, the contact zone is divided into elementary strips, the effective pressure on which is computed by simple integration of the elliptical pressure along the minor axis. Under prescribed operating conditions incremental traction so computed on the elementary strip is integrated along the major axis to estimate the total traction. The elastohydrodynamic film thickness is computed by formulae presented by Hamrock and Dowson[27] with appropriate correction for thermal effects per Wilson and Sheu.[28] This simplified treatment provides an adjustment to the film thickness to account for the thermal effects. The treatment is similar to the effect of shear stress on film thickness as discussed by Bair et al.[29] The effect of lubricant starvation may also be implemented using the model presented by Wolveridge et al.[30] However, the present investigation is directed toward turbine engine bearings, where the bearing is lubricated by circulating oil and the contacts are flooded with lubricant. Thus, no starvation effects are necessary in the present work. The change in film thickness, resulting from all operating mechanisms, affects traction in the contact zone, which in turn affects the thermal dissipation in the contact. Since the isothermal film thickness is primarily associated with lubricant behavior in the inlet zone, the various adjustments to the film thickness imply that the effects of thermal effects in the inlet zone are included in the model in a simplified manner. Assuming that the heat generated in the lubricant film is transferred primarily via conduction, the simplified Newtonian traction model may be formulated in terms of the following fundamental equations

$$\text{Energy equation}: \quad K(p,T)\frac{\partial^2 T}{\partial z^2} = -\tau\dot{\gamma} \tag{3}$$

$$\text{Geometric compatibility}: \frac{\partial u}{\partial z} = \dot{\gamma}(\tau,p,T) \tag{4}$$

$$\text{Constitutive equation}: \dot{\gamma}(\tau,p,T) = \frac{\tau}{\mu(p,T)} \tag{5}$$

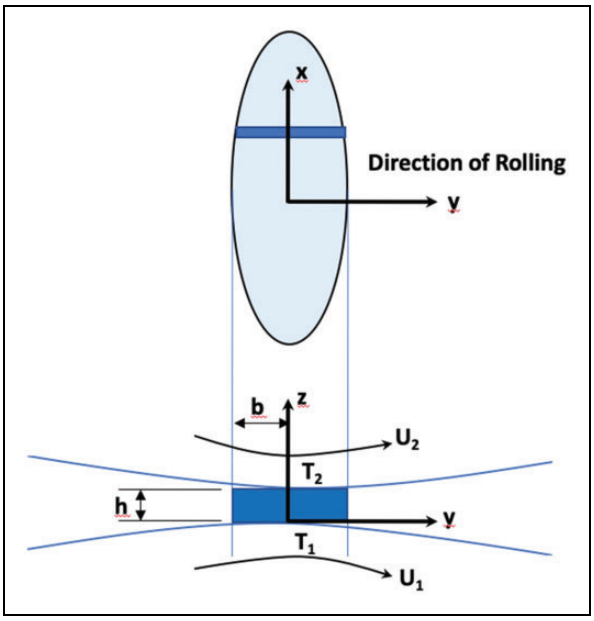

Figure 4. Schematic of a ball/race contact in a ball bearing.

Due to compressibility effects, the thermal conductivity, K, is pressure and temperature dependent. For the MIL-L-23699 lubricant, this variation is computed as per analysis presented by Bair.[31] Note that the energy equation (3) is primarily modeling losses due to lubricant shear under flooded conditions, as applicable to turbine engine bearings, and mixed lubricant is not modeled. Turbine engine bearings, the subject of primary focus in the present investigation, are invariably lubricated with circulating lubricant and the contacts are always fully flooded. Therefore, the assumptions in the above simplified formulation are realistic.

The applicable boundary conditions for the contact are

$$z = 0, \quad T = T_1 \quad \text{and} \quad u = U_1 \tag{6a}$$

$$z = h, \quad T = T_2 \quad \text{and} \quad u = U_2 \tag{6b}$$

Let T_o be a reference temperature at which the viscosity is μ_o; also, when $\mu = \mu_o$ the pressure $p = 0$.

With rolling velocity defined as

$$U = \frac{U_1 + U_2}{2}$$

define dimensionless variables

$$T^* = \frac{T}{T_o} \quad \mu^* = \frac{\mu}{\mu_o} \quad z^* = \frac{z}{h} \quad u^* = \frac{u}{U}$$

Equations (3) and (4) may be combined and after dropping the * may be written as

$$\frac{\partial^2 T}{\partial z^2} = -\frac{\tau U h}{K T_o}\frac{\partial u}{\partial z} \tag{7}$$

Likewise, equations (4) and (5) may be combined and written as

$$\frac{\partial u}{\partial z} = \frac{h\tau}{\mu_o \mu U} \tag{8}$$

Integrate equation (7) with boundary condition (6a) and then divide by equation (8) to obtain

$$\frac{1}{\mu}\frac{\partial T}{\partial u} = \frac{\mu_o U}{h\tau}\frac{\partial T}{\partial z}\bigg|_{z=0} - \frac{\mu_o U^2}{K T_o}(u - u_1) \tag{9}$$

Now integrate equation (9) with boundary conditions (6a) and (6b) to obtain

$$\int_{T_1}^{T_2} \frac{\partial T}{\mu} = \frac{\mu_o U}{h\tau}(u_2 - u_1)\frac{\partial T}{\partial z}\bigg|_{z=0} - \frac{\mu_o U^2}{K T_o}\int_{u_1}^{u_2}(u - u_1)\mathrm{d}u \tag{10}$$

where the terms under the integral on the right-hand side may be shown to be

$$\int_{u_1}^{u_2}(u - u_1)\mathrm{d}u = \frac{(u_2 - u_1)^2}{2} \tag{11}$$

Equation (11) may be substituted in equation (10) to compute $\frac{\partial T}{\partial z}\big|_{z=0}$, which may then be substituted in equation (10) to obtain the governing equation

$$\frac{1}{\mu}\frac{\partial T}{\partial u} = \frac{I}{u_2 - u_1} + \frac{\mu_o U^2}{K T_o}(1 - u) \tag{12}$$

where the integral I is

$$I = \int_{T_1}^{T_2} \frac{\mathrm{d}T}{\mu} \tag{13}$$

For rolling bearing contacts, a realistic specification of the temperatures at the film boundary requires more extensive thermal analysis of the system around the bearing, which is beyond the scope of the present investigation. However, if T_1 and T_2 are assumed to be equal, and the temperature distribution in the film is assumed to be symmetric with the maximum in the center, then the integral in equation (13) vanishes at all boundary temperatures. Thus, in the present investigation, an additional simplification is made by setting the temperatures at film boundary to be equal. The value of reference temperature, T_o, is then be set equal to this temperature to reduce the governing equation (12) to

$$\frac{\partial T}{\partial u} = \frac{\mu_o U^2}{K T_o}\mu(1 - u) \tag{14}$$

The above equation may now be numerically integrated with any arbitrary viscosity function, μ, to obtain temperature as a function of velocity u, which, with a prescribed viscosity relation, may be written in terms of viscosity variation as a function of velocity u. Using this variation of viscosity as a function of velocity, the applicable shear stress may be determined by integrating equation (8)

$$\tau = \frac{\mu_o U}{h}\int_{u_1}^{u_2} \mu \mathrm{d}u \tag{15}$$

Now if the velocity distribution through the film is assumed to be linear and since the temperatures at film boundary are already assumed to be equal, the temperature distribution through the film will be symmetric about the center of the film. Hence, equations (14) and (15) may only be integrated from film boundary to its center.

For rolling element to race contacts under high pressure and very low slide-to-roll ratios, as often encountered in most turbine engine bearings, Bair and Kotzalas[32] have shown that there is no difference between dry and viscous traction, and for accurate computation of traction, the applicable slide-to-roll ratio consists of slide-to-roll contribution from creep effects and the contribution from viscous effects. Under very low slide-to-roll ratios both the creep and viscous contribution to traction may be assumed to be linear with slide-to-roll. The creep slope may be approximated by the ratio of effective shear modulus to Hertz contact pressure while the viscous slope may be simply written in terms of Newtonian effects. Implementation of these effects for accurate computation of traction coefficient at very low slide-to-roll ratios is, therefore, quite straight forward.[32]

At high slide-to-roll ratios, which may only be encountered under excessive skidding in the bearing, a limiting shear must be implemented, as pointed out by Bair.[18] Based on available experimental data,[18] the ratio of this limiting shear to the contact pressure, or the limiting traction coefficient is set as 0.060.

Modeling of shear-thinning effects

The Carreau model as documented by Liu et al.,[26] perhaps, provides the simplest implementation of

shear-thinning effects in rolling bearing contacts. The effective shear stress, $\bar{\tau}$, for prescribed strain rate, $\dot{\gamma}$, and low shear Newtonian viscosity, μ, is written as one of the following relations

$$\bar{\tau} = \mu\dot{\gamma}\left[1 + \left(\frac{\mu}{G}\dot{\gamma}\right)^2\right]^{\frac{n-1}{2}} \tag{16}$$

or

$$\dot{\gamma} = \frac{\bar{\tau}}{\mu}\left[1 + \left(\frac{\bar{\tau}}{G}\right)^2\right]^{\frac{1-n}{2n}} \tag{17}$$

where G is the effective shear modulus and n is the shear-thinning exponent. When $n > 0.60$ both equations provide similar results.

From the geometric compatibility equation (4) and the Newtonian constitutive equation (5), the effective low shear Newtonian viscosity is related to computed Newtonian traction as

$$\tau = \mu\dot{\gamma} \tag{18}$$

Thus, by combining equations (16) and (18) the effective shear stress, as a result of shear-thinning effect, may be written as

$$\bar{\tau} = \tau\left[1 + \left(\frac{\tau}{G}\right)^2\right]^{\frac{n-1}{2}} \tag{19}$$

Based on experimental data documented by Bair[18] for a number of lubricants, the effective shear modulus, G, for the MIL-L-23699 type lubricant, is estimated as 8 MPa, while the shear-thinning exponent, n, could vary from 0.30 to 0.60. However, at high pressures, as encountered in turbine engine bearings, there may not be any significant shear-thinning effects. Therefore, the exponent n is estimated as 0.625, which is at the high end of the expected range.

Integrated traction in a contact and model validation

The above formulation provides incremental shear stress over an elementary strip at a grid point on the major contact axis in a ball/race contact or along the roller length in a roller/race contact. The slip is along the rolling direction but may vary along the contact length. For computation of total traction, this incremental shear stress is integrated over the length of the contact which may then be divided by the applied contact load, Q, to estimate an overall traction coefficient, κ

$$\kappa = \frac{1}{Q}\int_{-a}^{a} b(x)\bar{\tau}\mathrm{d}x \tag{20}$$

where a is the major contact half width in a ball bearing or half-length of roller in roller bearing.

Traction predictions at a contact stress of 2 GPa and at a rolling velocity of 22.5 m/s are compared with available experimental traction data in Figure 5, where the traction coefficient is plotted as a function of slide-to-roll ratio. The slide-to-roll ratio is defined as the ratio of slip velocity to the rolling velocity, which is the mean of the entraining velocity of

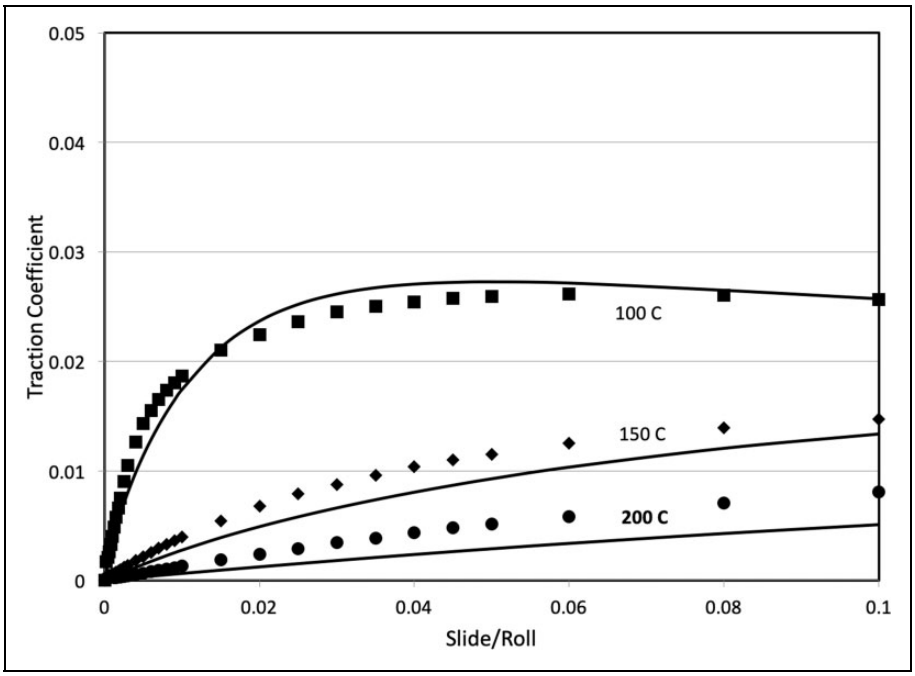

Figure 5. Newtonian/shear-thinning traction model validation against experimental data for 23699 lubricant with 2 GPa contact pressure and 22.5 m/s rolling velocity.

the two interacting surfaces. Clearly, the model predictions are fairly good. The only uncertainty in the model is the shear-thinning exponent n set at a value of 0.625. However, at a contact stress of 2 GPa, there is essentially no difference in traction predictions between $n = 0.625$ and $n = 1.0$, which represents no shear thinning. Thus, the speculation that at high pressure shear-thinning effect may be minimum[18] is well validated and the value of $n = 0.625$ is reasonable. Hopefully, as more experimental data become available in the future, a better correlation between the contact pressure and the shear-thinning exponent may be established.

Churning and drag model

In turbine engine applications, the circulating lubricant is constantly pumped through the bearing and the bearing elements, such as the rolling element and cage, have to move through the lubricant as they travel around the bearing; the process results in substantial drag force and churning moment on the bearing elements. Therefore, power dissipation in lubricant churning and drag effect generally constitutes a major fraction of overall heat generated in rolling bearings used in turbine engines. Unfortunately, precise definition of fluid flow around the bearing elements in a rolling bearing is a very complex and difficult task. Even with the fairly sophisticated tools, such those based on computational fluid dynamics, a number of simplifying assumptions are necessary to formulate any form of a model. Due to such modeling difficulties, the greatly simplified models formulated by Rumbarger et al.[2] still remain the current state-of-the-art in modeling of churning and drag losses. These models are based on classical laminar and turbulent fluid flow over spherical and cylindrical bodies as documented by Schlichtig.[3] The models are also implemented in the bearing dynamics code, ADORE, which constitutes the base model for the current investigation. The applicable equations for computing the drag forces and churning moments on the rolling elements and bearing cages are although fairly well documented in the available literature, they are summarized in Appendix 1 for completeness.

In most rolling bearings since the entire bearing cavity is not filled with lubricant, it is really a mixture of oil and air which constitutes the fluid media through which the rolling elements and cage move as they travel around the bearing. The simplified model assumes a homogeneous air–oil mixture with an input effective density and viscosity. Assuming that the density of air is negligible in comparison to that of the oil, the effective density of the fluid media is simply set as the lubricant density multiplied by the fraction of bearing cavity volume which is filled with the oil. For turbine engine bearings considered in the present work, a review of bearing geometries and the lubricant quantity supplied reveals that approximately 5% of bearing cavity is filled with oil. Thus, the effective density of churning and drag effects is 5% of lubricant density. For computing the shear forces as the rolling element and cage travel through the fluid media, the effective viscosity may be set equal to the lubricant viscosity with the assumption that the viscosity of air is negligible in comparison to that of the oil. For the MIL-L-23699 lubricant, this viscosity is simply derived from equation (1), developed above as a part of the traction model.

Modeling of thermal interactions

Implementation of thermal interactions in real-time rolling bearing performance simulations as obtained by integrating the classical differential equations of motion of bearing elements in time domain consists of several fundamental steps:

1. Computation of heat generation at a given time
2. Integration of thermal and mechanical time scales
3. Heat transport in the bearing and modeling of temperature fields
4. Modification of material properties, bearing geometry, and lubricant behavior as a function of temperature
5. Continued integration of equations of motion to steady-state behavior

At a given time the elements of heat generation consist of rolling element to race interactions, rolling element to cage contacts, cage to race contacts, and the power dissipated in lubricant churning and drag, as the bearing elements move through the circulating lubricant. For most rolling bearings under moderate applied load conditions, the majority of heat generation is due to lubricant churning and drag. These losses can be modeled by the simplified churning and drag models discussed above and summarized in Appendix 1. At a given time with prescribed loads and velocities, the elastohydrodynamic traction model discussed above provides the heat generated in the rolling element to race contacts. Both the rolling element and race contacts with the cage are high-speed sliding contacts subject to highly dynamic loads resulting from cage collisions with the bearing elements. Here a simple friction coefficient provides reasonable estimates of the frictional dissipations. Although the heat generated in these contacts is negligible in comparison to other sources, realistic modeling of cage contacts is significant in defining the cage motion and associated instabilities. Also, since the rolling element to cage contacts affect the rolling element velocity, these contacts have a direct impact on rolling element to race slip velocities, which in turn alter the thermal interactions at elastodydrodynamic rolling element to race contacts. All bearing elements are, therefore, intricately coupled. The general

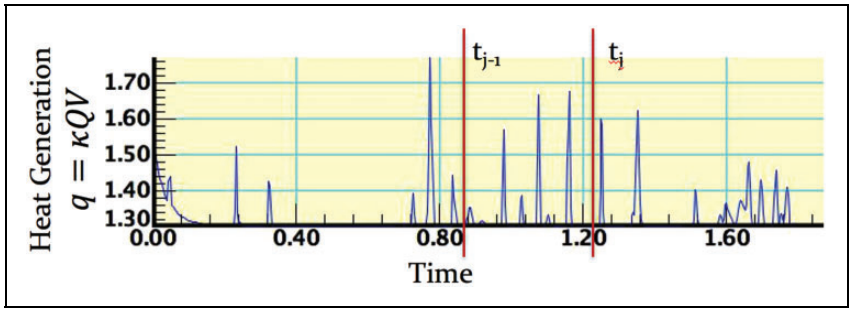

Figure 6. Schematic description of thermal averaging step in performance simulation time domain.

framework for such coupling between the various interactions is already available in the bearing dynamics computer code, ADORE,[9] which is the base model in the present investigation. Implementation of the updated traction models, as discussed above, in ADORE provides realistic modeling of lubricant traction and its role in overall bearing dynamics and heat generation.

As the differential equation of motion of bearing is integrated in time domain and simulation of bearing performance as a function of time continues, both the interacting load and temperature changes as a function of time are obtained until the bearing reaches steady-state operation. While the relative position of bearing elements is altered almost instantly as the loads change, the change in temperatures due to changing heat generations requires substantially larger time. Therefore, a simultaneous integration of the mechanical and thermal differential equations results in a very stiff system and integration over any reasonable time domain becomes extremely compute-intensive if not impractical. Therefore, a time-averaging algorithm to average out the heat generations, over a substantially large thermal time step, before the change in temperature field is computed, is implemented in the bearing dynamics computer code, ADORE.

As shown schematically in Figure 6 for a selected thermal step bounded by times t_{j-1} and t_j, the heat generation is averaged before applying a thermal analysis

$$\bar{q}_j = \frac{1}{\Delta t}\int_{t_{j-1}}^{t_j} q(t)\mathrm{d}t \tag{21}$$

where the thermal averaging step is defined as $\Delta t = t_j - t_{j-1}$.

The thermal averaging step is normally dependent on the transients in bearing element motion under prescribed operating conditions. Generally, a time interval corresponding to about 10 revolutions of the bearing is found to provide reasonable results.

Since the initial conditions for dynamic simulation of bearing performance are generally selected arbitrarily, the initial transients in the dynamic interactions may be insignificant. Therefore, these transients may be skipped before heat generation averaging is initiated for thermal analysis. Note that under stable operation, the steady-state solutions do not depend on initial conditions; the initial conditions may only control the time required to reach steady-state behavior.

Once the applicable heat generations at the various interfaces in the bearing are determined by the above step averaging approach, a thermal analysis is required to compute the temperature field in the bearing. Due to obvious complexities associated with heat flow in the bearing, such an analysis is generally very complex and perhaps the best approach may be to carry out a finite-element analysis. However, coupling of such an analysis with the time-varying solutions obtained by integrating the equations of motion of bearing elements further complicates the thermal analysis task. Thus, the thermal time-averaging model presented above is implemented to model the coupled thermal and dynamic performance of the bearing. Aside from lubricant churning and drag, the primary source of heat generation is the elastohydrodynamic contact between the rolling element and race. Depending on material properties of the races and rolling elements, heat generated at the rolling element to race contact is partitioned between rolling element and race. While the heat transferred to the rolling element travels to the circulating lubricant, portion of the heat transferred to the bearing race travels to the rest of the system. Since the overall system in which the bearing is mounted interacts with other system dependent components, the heat transferred to the races is simply left as model output, and the present investigation is restricted to just modeling the temperature fields in the bearing. With the simplified pattern of heat flow, schematically described in Figure 7, the model development in the current investigation is based on the following assumptions:

1. Heat generated at rolling element to race contact travels via conduction to the rolling element and race.
2. All heat transferred to the race goes to the support system and it is presently not modeled.
3. Heat generated at all cage contacts is transferred via conduction to the cage and contacting elements.
4. All heat transferred to the rolling elements and cage is transferred via convection to the circulating lubricant.

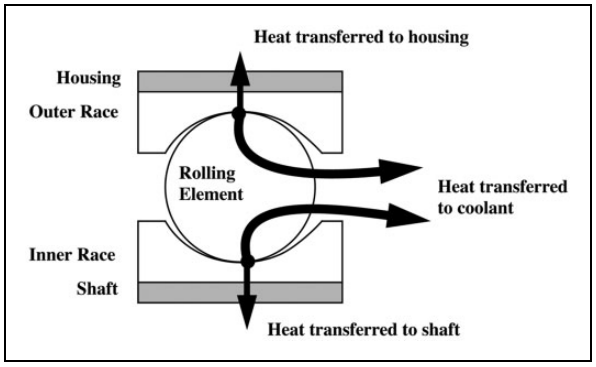

Figure 7. Schematic representation of heat transfer from primary load support contacts to the bearing races and external environment. For simplicity, the bearing cage is not shown in the schematic.

5. The heat generated due to churning and drag is added to the heat in the circulating fluid and travels out of the bearing.

All conduction type heat transfer is based on the simple conduction equation

$$q = -KA\frac{dT}{dx} \tag{22}$$

where q is the heat flux, K is the thermal conductivity, A is the effective area of flow, and dT/dx is the temperature gradient.

For the races, the contact heat generated at all the contacts with the rolling elements is summed and assumed to travel radially with the effective area defined by an equivalent cylindrical element corresponding to the race geometry. This permits computation of temperature gradient through the race in radial direction. For the rolling element, the bulk temperature is assumed to be average of the temperatures at outer and inner race contacts and the heat is assumed to be transferred to the circulating lubricant via convection.

Convective heat transfer is modeled as

$$q = hA(T_0 - T_\infty) \tag{23}$$

where T_0 is the surface temperature and T_∞ is the fluid temperature at exit. The applicable heat transfer coefficient, h, is estimated by available empirical relations for fluid flow past spherical and cylindrical bodies, as summarized in Appendix 2.

If $\mathcal{F}$ is the volumetric lubricant flow rate, and ρ and c_p are, respectively, the lubricant density and specific heat then the heat flux to circulating lubricant in terms of the inlet and exit temperatures is

$$q = \mathcal{F}\rho c_p(T_{exit} - T_{inlet}) \tag{24}$$

However, for the current MIL-L-23699 lubricant, both the density and specific heat are temperature dependent

$$\text{Density} : \rho = (1.009 - 0.0007296 \times T) \times 1000 \text{ kg/m}^3 \tag{25}$$

$$\text{Specific heat } c_p = (1763.2 + 2.4172 \times T)/1000 \text{ J/kg/K} \tag{26}$$

Also, part of the supplied lubricant may leak from the bearing. Therefore, the heat transferred to the circulating lubricant may be better defined in terms of the inlet and exit heat fluxes. Thus, if the fraction of lubricant quantity, which leaks out of the bearing, is χ, then the heat flux in the lubricant in the bearing at any temperature (T) is

$$q_{\mathcal{F}T} = \mathcal{F}(1 - \chi)\rho_T c_{pT} T \tag{27}$$

and the heat transferred to the lubricant as the lubricant exits from the bearing is written as

$$q_{\mathcal{F}} = q_{\mathcal{F}T_{exit}} - q_{\mathcal{F}T_{in}} \tag{28}$$

Since the experimental lubricant flow rate and input and exit temperatures are measurable with reasonable precision, experimental estimate of the heat transferred to the circulating fluid, as defined in equation (28), has the least uncertainty. It is, therefore, used to validate the model predictions.

As the integration of equation of motion continues in ADORE, the temperature fields are computed at each thermal step, over which the heat generations are averaged. The computed temperatures are then implemented as step change in temperature at various points in the bearing, and the material properties and bearing geometry are appropriately modified. While the material property database provides the applicable material properties at any temperature, the bulk temperature of bearing elements is used to compute thermal expansion and the resulting changes in internal bearing geometry. The integration continues until the step change in temperature becomes relatively insignificant and a steady-state condition is reached. The process is schematically outlined in Figure 8. An instability or thermal runoff is indicated when the operating temperatures do not converge to steady-state conditions and the change in computed temperatures keeps on increasing.

Experimental heat generation data and model validation

Since lubricant properties, bearing geometry, and operating conditions are fundamental inputs, the model may be used for any bearing. For the present investigation, three bearings, typical of turbine engine applications, all lubricated with the MIL-L-23699 lubricant, are considered. The first is an angular contact 160 mm ball bearing with M50-Nil VIMVAR

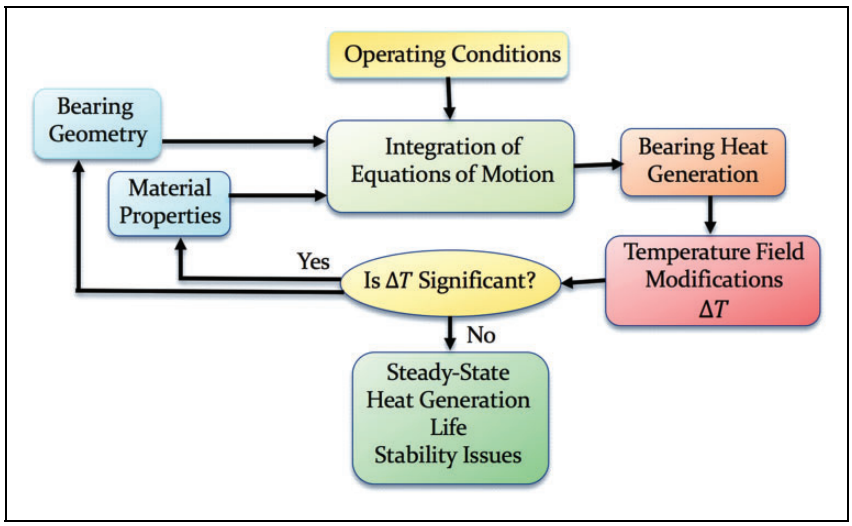

Figure 8. Schematic representation of thermal interaction analysis in ADORE.

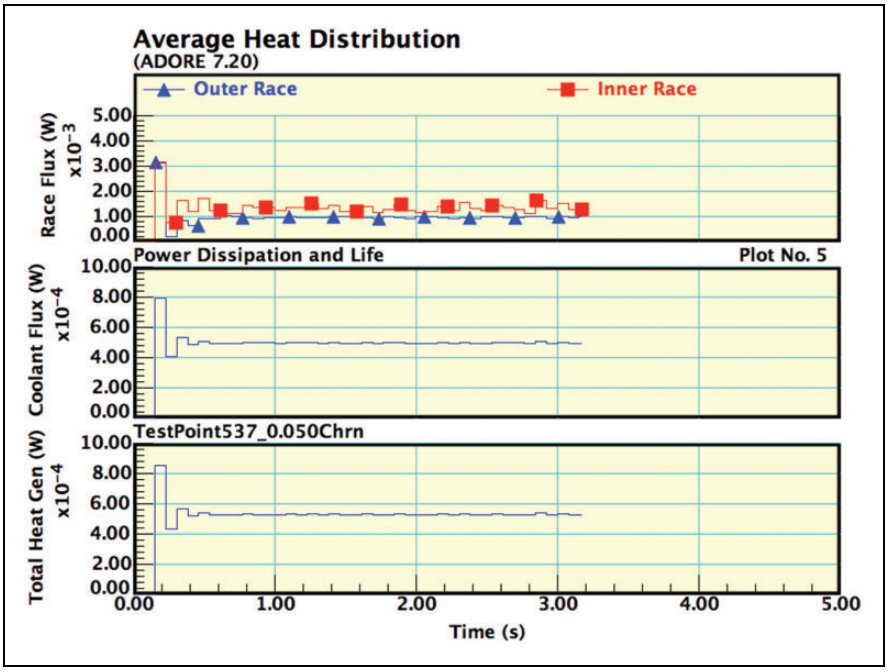

Figure 9. Typical heat fluxes as modeled at steady-state temperature fields.

races, M50 VIMVAR balls, and AISI 4340 steel cage with silver coating. Experimental data on this bearing are obtained as a part of a project at Rolls-Royce Corporation. The second bearing is the 133 mm angular contact ball bearing, used by Forster et al.[6,7]; the experimental heat generation data are available in the publications. Finally, experimental data on a 146.50 mm bore cylindrical roller bearing are also obtained at Rolls-Royce. This bearing also uses M50-NiL VIMVAR races, M50 VIMVAR rollers, and AISI 4340 steel cage with silver coating. Operating conditions for all bearings are typical of high-speed turbine engine applications.

Corresponding to a typical test point for 160 mm ball bearing, bearing heat generation solutions as obtained by ADORE are shown in Figure 9. Note that since the majority of heat generation is due to churning and drag losses, which are relatively insensitive to subtle dynamic variations in bearing element motion, the solution converges fairly rapidly to steady-state values. Heat flux to the coolant is the heat transferred to the lubricant as it circulates through the bearing. This quantity is validated against that determined for the experimental conditions using equations (24) to (28).

The step change in operating temperatures corresponding to the above bearing heat generation solution is plotted in Figure 10. The magnitude of step change in solutions reduces as the simulations approach steady-state conditions. Under unstable conditions

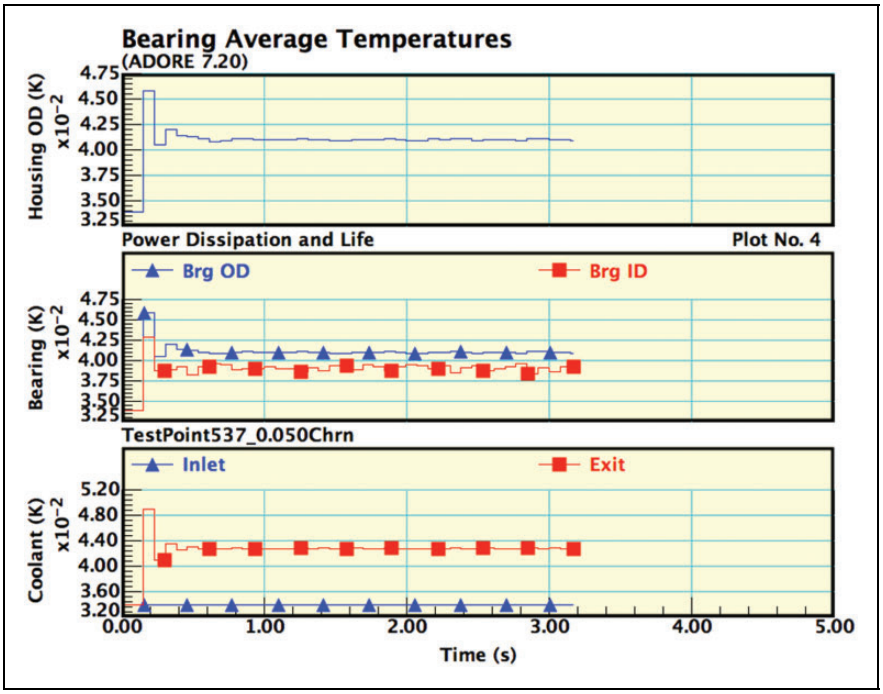

Figure 10. Bearing temperatures as modeled in ADORE for a typical test point.

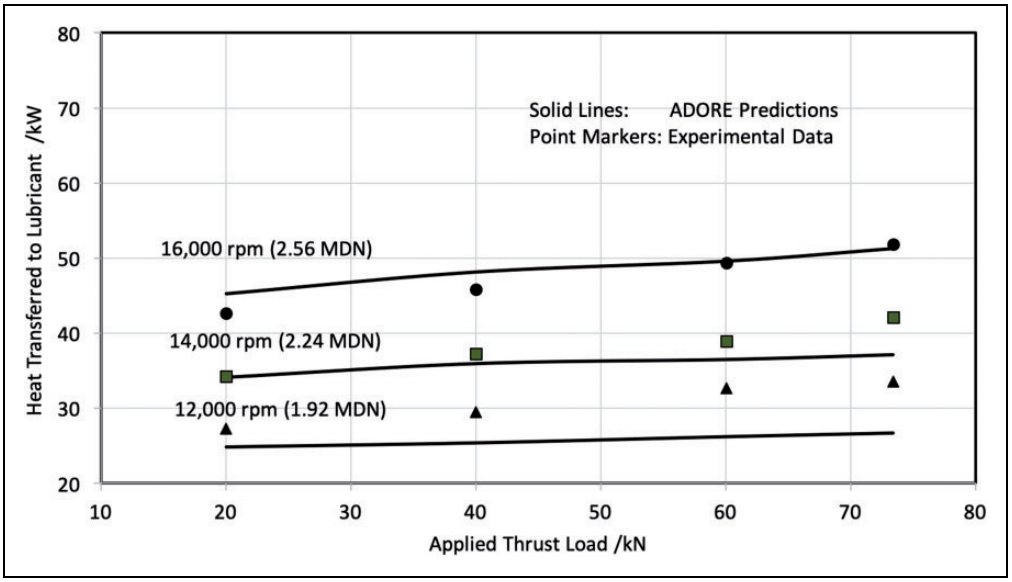

Figure 11. Validation of predicted heat transferred to the lubricant against experimental data for the 160 mm angular contact ball bearing with lubricant supply rate of 17.06 Lit/min at inlet temperature of 339 K.

this step change in solutions will progressively increase to indicate a thermal runoff condition.

All test bearings are under race lubricated and the lubricant is supplied by jets aimed at a scoop, from where the lubricant enters the bearing via lubricant holes in the inner race. The quantity of lubricant which misses the scoop, and does not make it to the bearing, is measured and it is defined as leaked lubricant. In all the tests, this quantity of lubricant is about 15% of the supplied lubricant. Over the entire range of experimental data, based on the quantity of lubricant supplied and the overall volume of the bearing cavity, the effective density of air–oil mixture in the bearing contributing to the churning and drag losses is estimated as 5% of lubricant density.

The predicted heat transferred to the lubricant is plotted against that measured experimentally for the 160 mm ball bearing over a range of operating conditions in Figure 11. At a given operating speed since the churning and drag losses are insensitive to load,

the load dependence of heat generation shown in Figure 11 is primarily contributed by the lubricant traction model.

While the predicted results agree fairly well with the experimental observations at high speed, there are some discrepancies at low speeds. Perhaps, the differences are related to the estimated quantity of lubricant in the bearing and the effective density of the lubricant at low speeds.

The 133 mm angular contact ball bearing considered in the present investigation is the one published by Forster et al.[6] along with experimental data on the inlet and exit lubricant temperature at the various operating conditions. The lubricant quantity, which leaks out the bearing, was not measured in these tests. Also, the range of experimental data is limited in comparison to that obtained in the present investigation for the 160 mm bearing. In view of these limitations, both the percentage of leaked lubricant and effective density for computing churning and drag losses are assumed to be same as those used for the 160 mm bearing. With these assumptions, the predicted heat transferred to the lubricant is validated against experimental data for 133 mm ball bearing in

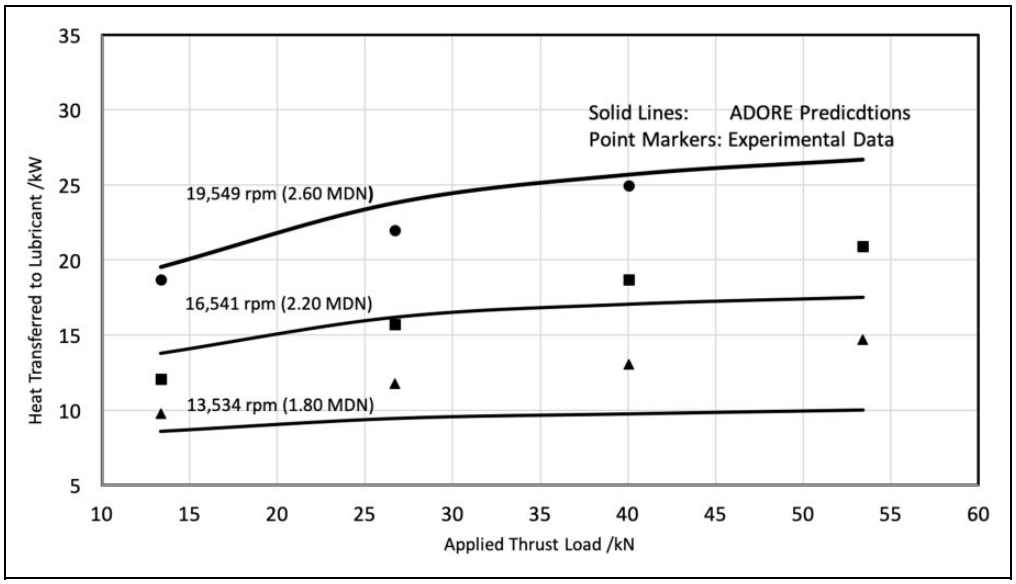

Figure 12. Validation of heat generation prediction against experimental data for the 133 mm bearing with lubricant supply rate of 11.40 Lit/min at inlet temperature of 394 K.

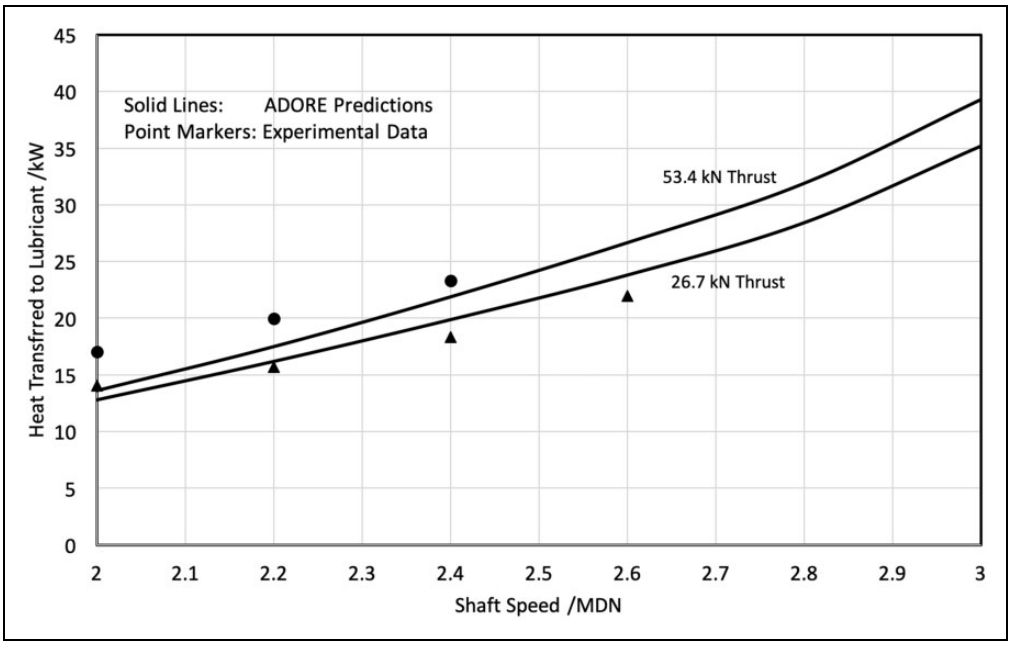

Figure 13. Validation of ADORE predictions of bearing heat generation against available experimental data for the 133 mm bearing with M50 balls, with lubricant supply rate of 11.40 Lit/min at inlet temperature of 394 K.

Figure 12. Again, the validations are fairly good at high speeds, while discrepancies at low speed are similar to those seen for 160 mm bearing.

Forster et al.[7] also tested a hybrid version of the 133 mm bearing, where the M50 balls are replaced by silicon nitride balls; the objective is to evaluate impact on bearing heat generation with ceramic rolling elements. Two sets of test data, one with M50 balls and the other with silicon nitride balls, under identical operating are published.[7] Corresponding to these test conditions, ADORE simulations are obtained to validate the model predictions. Again, in absence of any measurement of leaked lubricant and in view of limited test conditions, the fraction of leaked lubricant and effective lubricant density for modeling churning and drag effects are assumed to be the same as those used for the 160 mm bearing. For the M50 bearing, model predictions are validated against experimental data in Figure 13. Clearly, the model predictions are in reasonable agreement with measured experimental data.

Validations for hybrid version of the 133 mm bearing are shown in Figure 14. Since more than 90% of the predicted bearing heat generations, for both steel and hybrid bearings, is in churning and drag effects, which are relatively unchanged between all steel and

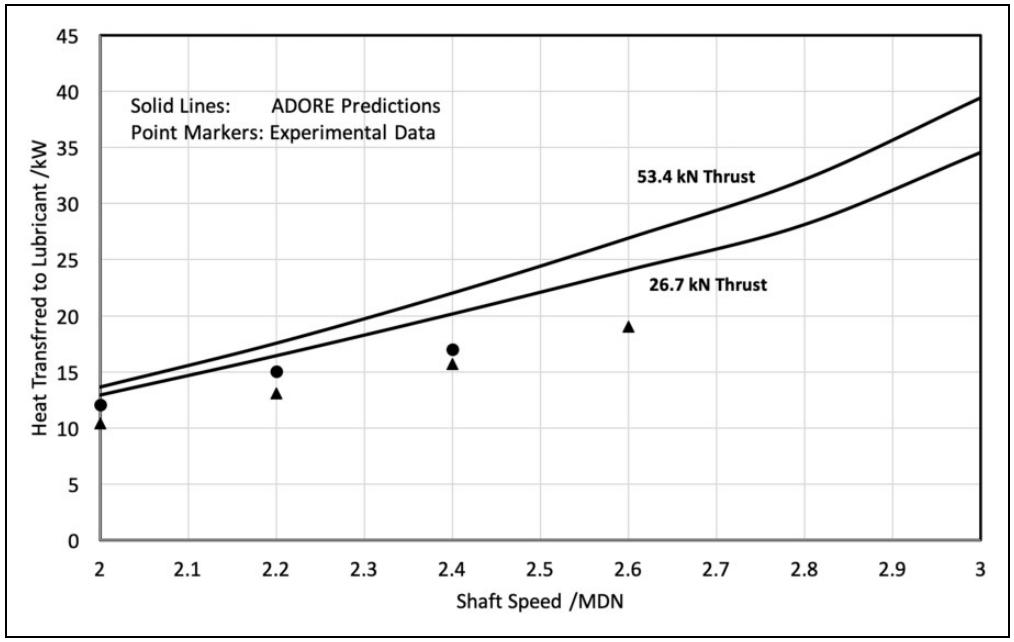

Figure 14. Comparison of ADORE predictions and available experimental data for the hybrid version of the 133 mm bearing with lubricant supply rate of 11.40 Lit/min at inlet temperature of 394 K.

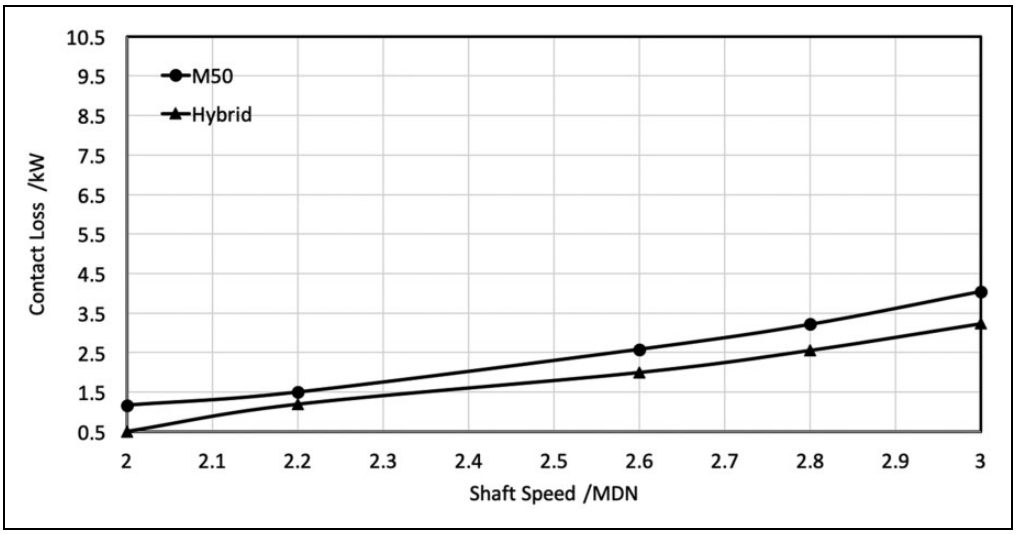

Figure 15. Contact heat generation comparison between M50 and hybrid 133 mm ball bearings at a light thrust load of 26.7 kN.

hybrid bearings, the predicted solutions are almost identical in Figures 13 and 14. However, the experimentally measured heat generation with the hybrid bearing is somewhat lower than that for the M50 bearing. While ADORE predictions better fit the M50 data, the predictions are higher for the hybrid bearing, although the trend of variation as a function of speed is similar between the predictions and experimental observations. This observation suggests that if the empirical effective density input in ADORE for modeling churning and drag is slightly reduced, the predictions will be very much in line with the experimental data; also, the overall heat generation predictions for the hybrid bearing will be lower as seen in the experimental data. In order to justify this adjustment, however, additional experimental support is necessary. Thus, more extensive measurement of lubricant flow in the 133 mm hybrid bearing is warranted. In view of these uncertainties, it is difficult to make a precise comparison between ADORE predictions and the limited experimental data available for the hybrid bearing.

For a prescribed load, hybrid bearing generally leads to a smaller ball/race contact area and higher contact stress. However, in angular contact ball bearings operating at high speed, the centrifugal loading at the ball/race contact is significantly lower with hybrid bearing; this affects both the contact load and angle. Therefore, the contact stress may not always be higher with the hybrid bearings. The contact heat generation, however, is always lower in hybrid bearings. This is generally not noticed in the overall heat generation in

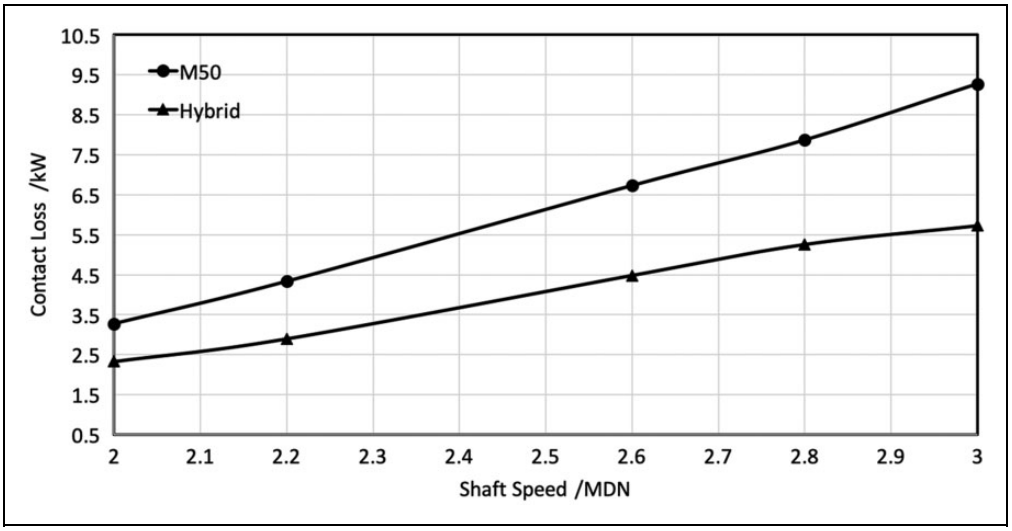

Figure 16. Contact heat generation comparison between M50 and hybrid 133 mm ball bearings under a heavy thrust load of 53.4 kN.

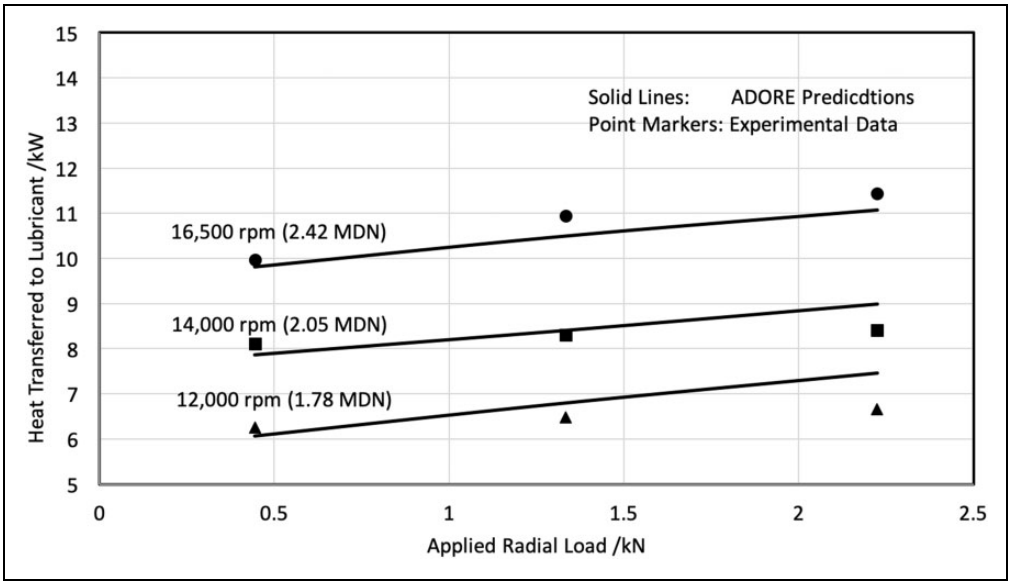

Figure 17. Validation of bearing heat generation prediction against experimental data for the 146.50 mm cylindrical roller bearing with lubricant supply rate of 6.62 Lit/min at inlet temperature of 339 K.

the bearing since the contact heat generation is often less than 10% of the total heat generation. At high speed and high loads, however, the contact heat generation may become a significant fraction of total heat generation. In order to evaluate such a speculation, two additional series of ADORE simulations for the M50 and hybrid bearing configuration are obtained with hypothetical elimination of any churning and drag losses. Bearing heat generations are then compared for the M50 and hybrid bearings. These results are shown, respectively, in Figures 15 and 16 for a light and heavy applied thrust load. Clearly, the heat generations in the hybrid bearing are notably lower in comparison to the M50 bearing; while the reduction in heat generation is about 20% at light load, it is close to 40% at the heavy load. Such an observation suggests a clear advantage of hybrid bearings for high-speed heavily loaded turbine engine bearings. It must, however, be remembered that bearing heat generation alters the temperature field in the bearing, which affects bearing geometry, material properties, and lubricant behavior. The thermal interaction models, as developed in the present investigation and implemented in ADORE, permit such coupled interactions and provide a thermally integrated dynamic simulation of bearing performance.

Experimental bearing heat generation data for the 146.50 mm cylindrical roller bearing, typical of turbine engine applications, are also obtained as part of a project at the Rolls-Royce. Measured quantity of lubricant, which leaked out of the bearing cavity, is again 15% of the supplied lubricant. Also, the effective density for modeling churning and drag losses is estimated as 5% of the lubricant density over the range of experimental data.

Similar to the ball bearing results, the validations for a cylindrical bearing are shown in Figure 17. Again, the agreement looks fairly good.

Summary

This investigation significantly enhances the bearing dynamics model, ADORE, to predict intricately coupled thermal behavior of rolling bearings. While the existing churning and drag models are used to compute lubricant churning and drag losses, the elastohydrodynamic traction model, for the rolling element to race contacts, is based on independently measured rheological behavior of the lubricant. In addition, the newly developed thermal model provides computation of time-varying temperature fields in the bearing, which affect both the operating bearing geometry and material properties. Integration of fundamental differential equations of motion of bearing element, under the time-varying bearing geometry and material properties, is continued to a steady-state condition until the temperatures stabilize to steady operating values.

Conventional elastohydrodynamic traction models based on constitutive equations, the coefficients of which are derived by regression analysis of actual traction data, are replaced by models based on independently measured lubricant rheology. Such models provide greatly improved traction predictions under turbine engine operating conditions, which are far beyond the experimental limits of traction rigs. The primary emphasis during the current development is on MIL-L-23699 type lubricant, commonly used in turbine engine applications. Following is a summary of accomplishments in the area of traction modeling:

1. A new traction model is based on independently measured viscosity–pressure–temperature behavior of the lubricant. The experimental viscosity data are correlated to Yasutomi-type relation, with thermal expansivity term as developed by Bair. This Yasutomi–Bair correlation provides viscosity predictions with greatly reduced uncertainty under arbitrary operating conditions.
2. With the prescribed viscosity–pressure–temperature equation, the energy equation is numerically integrated through the lubricant film to compute the temperature distribution and integrated Newtonian traction. The formulation provides reasonable modeling of thermal effects in the lubricant film.
3. Carreau-type model is used to apply shear-thinning effect on Newtonian traction. Thus, the model predictions include shear-thinning effects related to viscosity dependence on shear stress.
4. Traction predictions with the above model are in good agreement with independently measured traction-slip data.

While mechanical interaction between the bearing elements produces heat, the thermal interactions alter the temperature fields, which affect the bearing geometry and material properties, which, in turn, have an impact on mechanical interactions. Thus, bearing performance is dependent on close coupling between mechanical and thermal interactions. Following is a summary of results and findings of the current development effort:

1. While the classical differential equations of motion of all bearing elements are integrated in time domain, bearing heat generation at each time step is computed by summing all frictional dissipations in the bearing with the churning and drag losses. These transient solutions are time-averaged to compute average heat generation over the thermal time step. Thermal interaction analysis is then applied to compute the temperature field in the bearing and appropriate time-varying changes to bearing geometry and material properties are implemented. Integration of the differential

equations of motion then continues over the next time interval. In steady-state the process converges when the computed change in temperature field becomes insignificant. For high-speed turbine engine bearings, a thermal time step equivalent to about 10 revolutions of the bearing is found to be satisfactory for obtaining thermally integrated bearing performance simulations.
2. The steady-state bearing heat generation may be segmented into heat transferred to the circulating lubricant and that which goes to the housing and shaft systems. In an actual test, since the heat transferred to the circulating lubricant may be readily measured, comparison of predicted and measured values of these data provides a reliable model validation.
3. Heat generation predictions, as defined by heat transferred to the circulating lubricant, for a set of two angular contact ball bearings and a cylindrical roller bearing, typical of turbine engine applications, agree fairly well with experimentally measured data.
4. In a hybrid ball bearing, while the measured heat generation is somewhat lower than the corresponding all steel bearing, model predictions for both steel and hybrid bearing show no significant change in heat generation, although the trend of variation with operating speed is similar in both model prediction and experimental measurements. This is perhaps a result of the fact that more than 90% of total bearing heat generation is in lubricant churning and drag effects which are unchanged between steel and hybrid bearings.
5. To parametrically evaluate performance of the hybrid bearing in comparison to all steel bearing, additional performance simulations are obtained by suppressing the churning and drag effects. The contact heat generation, thus obtained, shows a 20% reduction at light load and almost 40% reduction at heavy load.

Declaration of Conflicting Interests

The author(s) declared no potential conflicts of interest with respect to the research, authorship, and/or publication of this article.

Funding

The author(s) disclosed receipt of the following financial support for the research, authorship, and/or publication of this article: Work reported in this article was carried out under US Air Force Small Business Innovation Research (SBIR) Phase II (Contract #FA8650-15-C-2534) contract awarded to PKG Inc. The Air Force Technical Contract Monitor was Jeremy Nickell, at Wright-Patterson Air Force Base, Ohio. The experimental data and related support were provided by Rolls-Royce Corporation, Indianapolis, Indiana. Extensive technical support in the development of traction model was provided by Dr Scott Bair at Georgia Institute of Technology.

References

1. Jones AB. A general theory for elastically constrained ball and radial roller bearings. *ASME Trans Ser D J Basic Eng* 1960; 82: 309–320.
2. Rumbarger JH, Filetti EG and Gubernick D. Gas turbine engine main shaft roller bearing system analysis. *ASME J Lubr Technol* 1973; 95: 401–416.
3. Schlichtig H. *Boundary layer theory*. New York: McGraw-Hill, 1968, pp.15–19, 93–99, 606–608.
4. Crecelius WJ and Pirvics J. *Computer program operation manual on SHABERTH a computer program for the analysis of the steady state and transient thermal performance of shaft-bearing systems*. Air Force AFAPL-TR-76-90, 1976, https://apps.dtic.mil/dtic/tr/fulltext/u2/a042981.pdf (accessed 15 April 2019).
5. Parker RJ. *Comparison of predicted and experimental thermal performance of angular contact ball bearing*. NASA TP-2275, 1984, https://ntrs.nasa.gov/search.jsp?R = 19840010586 (accessed 15 April 2019).
6. Forster NH, Svendsen VR, Givan GD, et al. Parametric testing and heat generation modeling of 133-mm bore ball bearings: part I – results with metal rolling elements. *Tribol Trans* 2011; 54: 315–324.
7. Forster NH, Svendsen VR, Givan GD, et al. Parametric testing and heat generation modeling of 133-mm bore ball bearings: part II – results with silicon nitride rolling elements. *STLE Tribol Trans* 2011; 54: 325–331.
8. Nicholson BD, Givan GD, Thompson KL, et al. Assessment of bearing heat generation prediction by the program ADORE with respect to experimental results and SHABERTH predictions. In: *Proc ASME turbo expo 2017: turbomachinery technical conference and exposition*, Charlotte, NC, 26–30 June 2017, paper no. GT2017-63010.
9. Gupta PK. *Advanced dynamics of rolling elements*. Berlin: Springer-Verlag, 1984.
10. Walters CT. The dynamics of ball bearings. *ASME Trans J Lubr Technol* 1971; 93: 1–10.
11. Gupta PK. Transient ball motion and skid in ball bearings. *ASME Trans J Lubr Technol* 1975; 97: 261–269.
12. Gupta PK. Dynamics of rolling element bearings. Parts I, II, II and IV. *ASME Trans J Lubr Technol* 1979; 101: 293–326.
13. Gupta PK. Current status of and future innovation in rolling bearing modeling. *STLE Tribol Trans* 2011; 54: 394–403.
14. Kannel JW and Walowit JW. Simplified analysis of tractions between rolling-sliding elastohydrodynamic contacts. *ASME J Lubr Technol* 1971; 93: 39–46.
15. Gupta PK, Flamand L, Berthe D, et al. On the traction behavior of several lubricants. *ASME Trans J Lubr Technol* 1981; 103: 55–64.
16. Johnson KL and Tevaarwerk JL. Shear behavior of elastohydrodynamic oil films. *Proc R Soc Lond Ser A* 1977; 356: 215–236.
17. Gupta PK, Cheng HS and Forster NH. Visco-elastic effects in MIL-L-7808 type lubricant, part I: analytical formulation. *STLE Tribol Trans* 1992; 35: 269–274.
18. Bair S. *High-pressure rheology for quantitative elastohydrodynamics*. Tribology and Interface Engineering Series 54, Editor B.J. Briscope, Amsterdam: Elsevier, 2007.
19. Bair S. A new high-pressure viscometer for oil/refrigerant solutions and preliminary results. *STLE Tribol Lubr Technol* 2017; 73: 60–70.

20. Yasutomi S, Bair S and Winer WO. An application of a free volume model to lubricant rheology: I. Dependence of viscosity on temperature and pressure. *ASME J Tribol* 1984; 106: 291–303.
21. Williams ML, Landel RF and Ferry JD. The temperature dependence of relaxation mechanisms in amorphous polymers and other glass-forming liquids. *J Am Chem Soc* 1955; 77: 3681–3934.
22. Bair S, Mary C, Bouscharain N, et al. An improved Yasutomi correlation for viscosity and high pressure. *Proc IMechE, Part J: J Engineering Tribology* 2013; 227: 1056–1060.
23. Campos A, Sottomayor A and Seabra J. Non-Newtonian thermal analysis of an EHD contact lubricated MIL-L-23699 oil. *Tribol Int* 2006; 39: 1732–1744.
24. Habchi W, Eyheramendy D, Bair S, et al. Thermal elastohydrodynamic lubrication of point contact using Newtonian/generalized Newtonian lubricant. *Tribol Lett* 2008; 30: 41–52.
25. Habchi W, Vergne P, Bair S, et al. Influence of pressure and temperature dependence of thermal properties of a lubricant on the behavior of circular TEHD contacts. *Tribol Int* 2010; 43: 1842–1850.
26. Liu Y, Wang J, Bair S, et al. A quantitative solution for the full shear-thinning EHL point contact problem including traction. *Tribology Letter* 2007; 28: 171–181.
27. Hamrock BJ and Dowson D. Isothermal elastohydrodynamic lubrication of point contacts, part III – fully flooded results. *ASME J Lubr Technol* 1977; 99: 264–276.
28. Wilson WRD and Sheu S. Effect of inlet shear heating due to sliding on elastohydrodynamic film thickness. *ASME J Lubr Technol* 1983; 105: 187–188.
29. Bair S, Vergne P and Marchetti M. The effect of shear-thinning on film thickness for space lubricants. *STLE Tribol Trans* 2002; 45: 330–333.
30. Wolveridge PE, Baglin KP and Archard JF. The starved lubrication of cylinders in line contact. *Proc Instn Mech Engrs* 1970–1971; 185: 1159–1169.
31. Bair S. Density scaling of thermal conductivity of a jet oil. *STLE Tribol Trans* 2014; 57: 647–652.
32. Bair S and Kotzalas M. The contribution of roller compliance to elastohydrodynamic traction. *STLE Tribol Trans* 2006; 49: 218–224.
33. McAdams WH. *Heat transmission*. New York: McGraw-Hill, 1954, pp.265–268.
34. Kreith F. *Principles of heat transfer*. 2nd ed. Scranton, PA: International Text Book Co., 1966, pp.410–415.
35. Rohsenow WH and Choi HY. *Heat mass and momentum transfer*. Englewood Cliffs, NJ: Prentice-Hall, 1961, pp.200–202.

Appendix

Notation

a	major contact half width (m)
ADORE	Advanced Dynamics of Rolling Elements
AISI	American Iron and Steel Institute
b	minor contact half width (m)
DN	Product of Bearing bore (mm) and shaft speed (RPM)
f	friction factor
$\mathcal{F}$	volumetric lubricant flow rate (m^3/s)
h	film thickness (m)
K	thermal conductivity (W/m/K)
MDN	Million DN
n	shear-thinning exponent
q	heat flux (W)
Q	contact load (N)
r	effective radius (m)
SHABERTH	A Computer Program for the Steady-State and Transient Analysis of Shaft Bearing Systems
T	temperature (K)
u	velocity (m/s)
U	rolling velocity (m/s)
VIMVAR	Vacuum Induction Melt, Vacuum Arc Remelt
α	pressure–viscosity coefficient (1/Pa)
β	temperature–viscosity coefficient (K or 1/K)
γ	pressure–temperature–viscosity coefficient (K/Pa)
$\dot{\gamma}$	strain rate (1/s)
κ	traction coefficient
μ	viscosity (Pa.s)
ρ	density (kg/m^3)
τ	shear stress (Pa)

Appendix 1. Simplified lubricant churning and drag models

The current state-of-the-art lubricant churning and drag model is based on the early work of Rumbarger et al.[2] The model equations for drag forces and churning moments presented below are based on classical laminar and turbulent flow as documented by Schlichtig.[3]

Drag forces on ball and rollers in rolling bearings are generally estimated in terms of drag coefficients for spherical and cylindrical bodies

$$F_D = C_D\left[\frac{1}{2}\rho V^2 \mathrm{A}\right] \tag{29}$$

where C_D is the drag coefficient, the experimentally measured values of which are documented by Schlichtig[3]; ρ is the effective density; V is the orbiting velocity; A is the frontal area; and F_D is the computed drag force. The frontal area on the rolling element is the area subjected to drag; this is simply the rolling element face area minus the area covered by the cage. The drag coefficient is generally tabulated as a function of Reynolds number, Re

$$Re = \frac{\rho V d}{\mu} \tag{30}$$

Here d is a characteristic length, which is the rolling element diameter and μ is the lubricant viscosity. For completeness the drag coefficients for spherical and

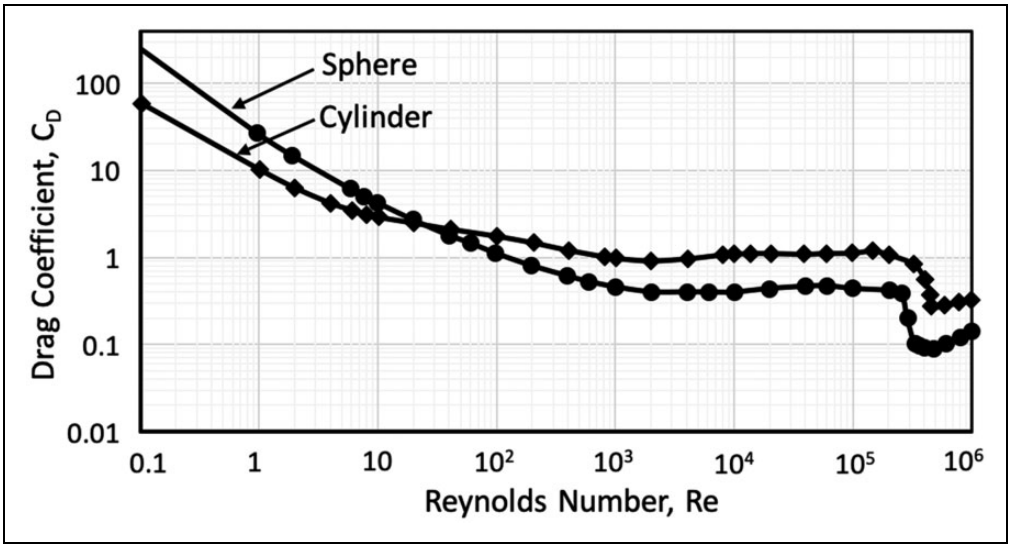

Figure 18. Drag coefficients for spherical and cylindrical bodies as documented by Schlichtig.[3]

cylindrical bodies, as reported by Schlichtig,[3] are plotted in Figure 18.

The resulting power loss due to this drag is simply the drag force multiplied by the orbital velocity.

Churning moments are significant for rollers and the cage. Normally, there is a loss on both the cylindrical surfaces and end faces. An empirical formula for moment on the cylindrical surface is written as

$$M_c = \frac{1}{2} f \rho U^2 \mathrm{A} r \tag{31}$$

Here ρ is the applicable density, A is the area, r is a reference radius from center of rotation, U is the mass average velocity of fluid, and the friction factor, f is defined as follows

$$\text{Vortex turbulent flow}: \ \frac{f}{f_L} = 1.3\left(\frac{Ta}{41}\right)^{0.539474}\Bigg|_{Ta>41} \tag{32a}$$

$$\text{Couette turbulent flow}: \ \frac{f}{f_L} = 3.0\left(\frac{Re}{2500}\right)^{0.85596}\Bigg|_{Re>2500} \tag{32b}$$

$$\text{Laminar friction factor}: \ f_L = \frac{16}{Re}\Bigg|_{Re<2500 \text{ or } Ta<41} \tag{32c}$$

$$\text{Reynolds number}: \ Re = \frac{\rho r \omega c}{\mu} \tag{32d}$$

$$\text{Taylors number}: \ Ta = \frac{\rho r \omega c}{\mu}\sqrt{\frac{c}{r}} \tag{32e}$$

Generally, the reference radius, r, is the radius of the rotating cylindrical surface; and c is the effective clearance between the rotating cylindrical surface and stationary housing. For rollers in a cage pocket, the pocket clearance may be used.

For typical high-speed roller bearings, the flow on cage surface is approximated as Couette turbulent, while the vortex turbulent flow is assumed for the roller surface.

For the end surfaces of the cage, as well as roller ends, the churning moment is written as

$$M_c = \frac{1}{2}\rho\omega^2 r^5 C_n \tag{33a}$$

$$C_n = 3.87/Re^{0.50} \text{ for laminar flow } Re < 300,000 \tag{33b}$$

$$C_n = 0.146/Re^{0.20} \text{ for turbulent flow } Re > 300,000 \tag{33c}$$

$$Re = \frac{\rho r^2 \omega}{\mu} \text{ is the Reynolds number} \tag{33d}$$

The effective radius, r, for roller is simply the roller radius, but for the cage, which has the inner and outer radius, r_{in} and r_{out}, respectively, the effective radius is estimated as

$$r^5 = r_{out}\left(r_{out}^4 - r_{in}^4\right) \text{ for laminar flow} \tag{34a}$$

$$r^5 = r_{out}^{0.40}\left(r_{out}^{4.60} - r_{in}^{4.60}\right) \text{ for turbulent flow} \tag{34b}$$

Although no explicit expressions for computing churning moment on the ball are available, the moment is approximated by that occurring on a projected area normal to the ball angular velocity, which

approximates it as a thin disk, with no cylindrical surface. Thus, equation (33) is used.

The churning loss is simply the product of computed churning moment and applicable angular velocity of rotation.

Appendix 2. Convective heat transfer coefficients in rolling bearings

Convective heat transfer coefficient related to lubricant flow past the bearing elements may be estimated from the available empirical solutions for fluid flow past spherical and cylindrical bodies.[33–35] These solutions are expressed in terms of the following three dimensionless groups

$$\text{Reynolds number}: \ Re = \frac{\rho V D}{\mu} \tag{35a}$$

$$\text{Prandtl number}: \ Pr = \frac{\mu c_p}{K} \tag{35b}$$

$$\text{Nusselt number}: \ Nu = \frac{hD}{K} \tag{35c}$$

Here ρ, V, μ, c_p, K, D, and h are, respectively, the fluid density, velocity, viscosity, specific heat, thermal conductivity, characteristic length of the solid, and the applicable heat transfer coefficient.

Pertinent to rolling bearings the solids of interest are spheres and cylinders and the fluid of interest is the liquid lubricant. Thus, for ball bearings, the applicable equation of spheres[35] in liquid is

$$\text{Spheres in liquid}: \ Nu = Pr^{0.30}\left[0.97 + 0.68\sqrt{Re}\right] \tag{36}$$

In the limiting case, with $Re < 1$ and $Pr = 1$, the Nusselt number approaches a value of 2.

A similar expression for cylinders[35] in liquid, which may be applied to roller bearings is

$$\text{Cylinders in liquid}: \ Nu = Pr^{0.31}\left[0.35 + 0.56\sqrt{Re}\right] \tag{37}$$

The Reynolds number, as applicable to the rolling elements (ball or roller), is based on the rolling element orbital velocity. Although the cage, essentially driven by the rolling elements, is a cylindrical element, most of the convection is controlled by fluid flow through the pockets, which is quite complex. Therefore, the Nusselt number for the cage is set equal to that computed for the rolling elements.